

Antenna Switching Sequence Design for Channel Sounding in a Fast Time-varying Channel

Rui Wang¹, *Student Member, IEEE*, Olivier Renaudin^{1,2}, *Member, IEEE*, C. Umit Bas¹, *Student Member, IEEE*,
Seun Sangodoyin¹, *Student Member, IEEE*, Andreas F. Molisch¹, *Fellow, IEEE*

¹University of Southern California, Los Angeles, CA USA

²Austrian Institute of Technology, Vienna, Austria

Abstract—This paper investigates the impact of array switching patterns on the accuracy of parameter estimation of multipath components for a time division multiplexed (TDM) channel sounder. To measure a fast time-varying channel, the conventional uniform array switching pattern poses a fundamental limit of the number of antennas that a TDM channel sounder can utilize. We propose a method, which is based on simulated annealing, to find non-uniform array switching patterns for realistic antenna arrays, so that we can extend the Doppler estimation range of the channel sounder by suppressing the high sidelobes in the spatio-temporal ambiguity function. Monte Carlo simulations demonstrate that the optimal switching sequence leads to significantly smaller root mean square errors of both direction of departure and Doppler. Results can be applied in both vehicle-to-vehicle and millimeter wave MIMO channel measurements.

I. INTRODUCTION

Realistic radio channel models are essential for development and improvement of communication transceivers and protocols [1]. Realistic models in turn rely on accurate channel measurements. Various important wireless systems are operating in fast-varying channels, such as millimeter wave (mmWave), vehicle-to-vehicle (V2V) and high speed railway systems. The need to capture the fast time variations of such channels creates new challenges for the measurement hardware as well as the signal processing techniques.

Since most modern wireless systems use multiple antennas, channel measurements also have to be done with multiple-input multiple-output (MIMO) channel sounders. There are three types of implementation of such sounders: (i) full MIMO, where each antenna element is connected to a different RF chain, (ii) virtual array, where a single antenna is moved mechanically to emulate the presence of multiple antennas, and (iii) switched array, also known as time-division multiplex (TDM) sounding, where different physical antenna elements are connected via an electronic switch to a single RF chain. The last configuration is the most popular in particular for outdoor measurements, as it offers the best compromise between cost and measurement duration.

From measurements of MIMO impulse responses or transfer functions, it is possible to obtain the parameters (direction of departure (DoD), direction of arrival (DoA), delay, and complex amplitude) of the multipath components (MPCs) by means of high resolution parameter estimation (HRPE) algorithms. Most HRPE algorithms are based on the assumption

that the duration of one MIMO snapshot (the measurement of impulse responses from every transmit to every receive antenna element) is shorter than the coherence time of the channel. Equivalently, this means the MIMO cycle rate, i.e. the inverse of duration between two adjacent MIMO snapshots, should be greater than or equal to half of the maximal absolute Doppler shift, in order to avoid ambiguities in estimating Doppler shifts of MPCs. Since in a switched sounder the MIMO snapshot duration increases with the number of antenna elements, there seems to be an inherent conflict between the desire for high accuracy of the DoA and DoD estimates (which demand a larger number of antenna elements) and the admissible maximum Doppler frequency.

Yin *et al.* were first to realize that it was the choice of uniform array switching patterns that causes this limit in TDM channel sounding [2]. A non-uniform array switching pattern can potentially significantly extend the estimation range of Doppler shifts and eliminate the ambiguities. They studied the problem in the context of the ISI-SAGE algorithm [3]. However their analysis not only assumes that all antenna elements are isotropic radiators, but also requires the knowledge of the phase centers of all antennas. Both assumptions are difficult to fulfill for realistic arrays used in a channel sounder, given the mutual coupling between antennas and the presence of a metallic support frame. Pedersen *et al.* proposed to use the so-called normalized sidelobe level (NSL) of the objective function as the metric to identify switching patterns [4]. They further derived a necessary and sufficient condition of the array switching sequence that leads to ambiguities [5], but the method to design a good switching sequence is not clear. To our best knowledge, no methods have been proposed to find optimized switching patterns for realistic arrays.

Our work adopts an algebraic model that uses decompositions through effective aperture distribution functions (EADFs) [6], which provides a reliable and elegant approach for signal processing with real-world arrays. Therefore our analysis no longer requires the isotropic radiation pattern or prior knowledge about the antenna phase centers. Based on the Type I ambiguity function for an arbitrary array [7], we propose a spatio-temporal ambiguity function and investigate its properties and impact on the estimation of directions and Doppler shifts of MPCs. Inspired by Ref. [8], we model the array pattern design problem as an optimization problem and propose an algorithm based on simulated annealing (SA) to

search for an acceptable solution. The results are validated with Monte-Carlo simulations when the final switching sequence is incorporated into a RiMAX-based HRPE algorithm.

The remainder of the paper is organized as follows. Section II introduces the signal data model in TDM channel sounding and the spatio-temporal ambiguity function. In Section III we present the formulation of the optimization problem and its solution based on the SA algorithm. In Section IV we demonstrate the performance of the optimal switching sequence with a corresponding HRPE algorithm, and compare root mean squared errors (RMSEs) of key parameters with the squared root of Cramer-Rao lower bound (CRLB). In Section V we draw the conclusions.

II. SIGNAL MODEL AND AMBIGUITY FUNCTION

A. Signal Data Model

This work mainly studies the antenna switching sequence in the TDM channel sounding problem. We consider T MIMO measurement snapshots in one observation window, each with M_f frequency points, M_R receive antennas, and M_T transmit antennas. The adjacent MIMO snapshots are separated by T_0 . We assume that all scatterers are placed in the far field of both transmitter (TX) and receiver (RX) arrays, which also implies that MPCs are modeled as plane waves. Besides TX and RX arrays are vertically polarized by assumption and have frequency-independent responses within the operating bandwidth. Such T MIMO snapshots can span larger than the coherence time of the channel, but we assume that the large-scale parameters of the channel, such as path delay, DoA, DoD and Doppler shift, remain constant during this period.¹

A *vectorized* data model for the observation of T MIMO snapshots is given in Eq. (1). It includes contributions from deterministic specular paths (SPs) $\mathbf{s}(\boldsymbol{\theta}_{sp})$, diffuse multipath components (DMC) \mathbf{n}_{dmc} and measurement noise \mathbf{n}_0 .

$$\mathbf{y} = \mathbf{s}(\boldsymbol{\theta}_{sp}) + \mathbf{n}_{dmc} + \mathbf{n}_0 \quad (1)$$

The data model of a observation vector for a total number of P SPs is determined by

$$\mathbf{s}(\boldsymbol{\theta}_{sp}) = \mathbf{B}(\boldsymbol{\mu}) \cdot \boldsymbol{\gamma}_{vv}, \quad (2)$$

where $\boldsymbol{\gamma}_{vv}$ is a vector of the complex path gains, $\boldsymbol{\mu}$ is the structural parameter vector, and $\mathbf{B}(\boldsymbol{\mu})$ is the basis matrix. The detailed structure of $\mathbf{B}(\boldsymbol{\mu})$ when a uniform switching pattern is used can be found in [9, Eq. (20)]. $\boldsymbol{\theta}_{sp}$ is the entire parameter vector for SPs, thus includes both $\boldsymbol{\mu}$ and $\boldsymbol{\gamma}_{vv}$.

We would like to incorporate the choice of non-uniform switching patterns into this signal data model. To facilitate the implementation of the associated HRPE algorithm, we only allow the TX array to implement a cycle-dependent switching pattern, while the RX array's switching pattern

remains uniform. As a result the basis matrix can be expressed as

$$\mathbf{B}(\boldsymbol{\mu}) = \tilde{\mathbf{B}}_{TV,T} \diamond \tilde{\mathbf{B}}_{RV} \diamond \mathbf{B}_f \quad (3)$$

$$= \left[\tilde{\mathbf{B}}_{TV}^1 \quad \dots \quad \tilde{\mathbf{B}}_{TV}^T \right]^T \diamond \tilde{\mathbf{B}}_{RV} \diamond \mathbf{B}_f, \quad (4)$$

where $\mathbf{B}_{TV}^j \in \mathbb{C}^{M_T T \times P}$ with $j = 1, 2, \dots, T$ represents the spatio-temporal response of TX array at the j -th MIMO snapshot, and $\tilde{\mathbf{B}}_{RV} \in \mathbb{C}^{M_R \times P}$ is for the RX array with uniform switching, and $\mathbf{B}_f \in \mathbb{C}^{M_f \times P}$ is the basis matrix that captures the frequency response due to path delay. Compared with the basis matrix in [9, Eq. (20)], we replace $\mathbf{B}_t \diamond \tilde{\mathbf{B}}_{TV}$ with $\tilde{\mathbf{B}}_{TV,T}$ due to the scrambled switching sequence allowed at the TX array.

Since our work focuses on channel sounding in a fast time-varying channel, the phase variation within one MIMO snapshot is no longer negligible, and the new TX or RX basis matrices for the t -th MIMO snapshot become weighted versions of the static array basis matrices. The exact connections are given by

$$\tilde{\mathbf{B}}_{TV}^t = \mathbf{B}_{TV} \odot \mathbf{A}_T^t \quad (5)$$

$$\tilde{\mathbf{B}}_{RV} = \mathbf{B}_{RV} \odot \mathbf{A}_R, \quad (6)$$

where \mathbf{A}_R and \mathbf{A}_T^t are weighting matrices that capture the phase change due to effects of Doppler and switching schemes. \mathbf{A}_T^t depends on the MIMO snapshot index t , because TX implements a cycle-dependent switching pattern. Let us use a $M_T \times T$ matrix $\boldsymbol{\eta}_T$ to represent the TX switching pattern, the elements in the phase weighting matrices \mathbf{A}_T^t and \mathbf{A}_R are given by

$$[\mathbf{A}_T^t]_{m_T,p} = e^{j2\pi\nu_p[\boldsymbol{\eta}_T]_{m_T,t}} \quad (7)$$

$$[\mathbf{A}_R]_{m_R,p} = e^{j2\pi\nu_p m_R t_0}. \quad (8)$$

If we maintain the duration between two adjacent switching events for both TX and RX array, and denote them as t_1 and t_0 respectively, we have

$$[\boldsymbol{\eta}_T]_{m_T,t} = (t-1)M_T t_1 + ([\mathbf{S}_T]_{m_T,t} - 1)t_1 \quad (9)$$

$[\mathbf{S}_T]_{m_T,t}$ takes an integer value between 1 and M_T and represents the scheduled switching index of the m_T th TX antenna for the t th MIMO snapshot. For example with the uniform switching pattern, we have $[\mathbf{S}_T]_{m_T,t} = m_T, \forall t = 1, 2, \dots, T$.

B. Spatio-temporal Ambiguity Function

The Type I ambiguity function for an antenna array can reflect its ability to differentiate signals in the angular domain [7]. Generalizing the definition to include the full parameter vectors employed in our model, we have

$$X_{tot}(\boldsymbol{\mu}_1, \boldsymbol{\mu}_2) = \frac{\mathbf{b}(\boldsymbol{\mu}_1, \boldsymbol{\eta}_T)^\dagger \mathbf{b}(\boldsymbol{\mu}_2, \boldsymbol{\eta}_T)}{\|\mathbf{b}(\boldsymbol{\mu}_1, \boldsymbol{\eta}_T)\| \cdot \|\mathbf{b}(\boldsymbol{\mu}_2, \boldsymbol{\eta}_T)\|}, \quad (10)$$

where $\boldsymbol{\mu}_1$ or $\boldsymbol{\mu}_2$ stands for the structural parameter vector of one SP. $\mathbf{b}(\boldsymbol{\mu}_1, \boldsymbol{\eta}_T)$ can be treated as one particular column of $\mathbf{B}(\boldsymbol{\mu})$.

¹This does not indicate the channel is assumed to be static, the complex path weight of SP have a phase rotation due to the presence of Doppler shift.

This multi-dimensional ambiguity function is also closely related to the ambiguity function well studied in MIMO radar. The MIMO radar ambiguity function in Ref. [8] allows the TX to send different waveforms on different antennas, while our problem considers a single sounding waveform for all TX antennas. The Doppler-(bi)direction ambiguity function used in Ref. [5] is also quite similar to ours, except that we work with the channel transfer function instead of the received waveform. Moreover they assume that the array is composed of identical elements and suffers no mutual coupling effects, our ambiguity function is more general in the sense that it handles various array structures.

Additionally instead of directly evaluating the ambiguity function in Eq. (10), we can find an upper bound for its amplitude, which merely depends on the azimuth DoD, the Doppler shift, and the TX switching pattern. Our work considers a switched array setup in a fast time-varying channel, and the measurement spans both spatial and temporal domain, so it is natural to focus on two dimensions, namely azimuth DoD and Doppler. We call the simplified 2D ambiguity function the spatio-temporal ambiguity function, and its relation with the generalized ambiguity function of Eq. (10) is given as

$$|X_{tot}(\boldsymbol{\mu}, \boldsymbol{\mu}')| \leq |X_T(\varphi_T, \varphi'_T, \nu, \nu')|. \quad (11)$$

Detailed derivations about this inequality and associated properties of this spatio-temporal ambiguity function are included in Ref. [10]. Furthermore we can show that this upper bound only depends on the difference of two Doppler shifts, *i.e.* $\Delta\nu = \nu' - \nu$, which is given by

$$X_T(\varphi_T, \varphi'_T, \nu, \nu') = \frac{\tilde{\mathbf{b}}_{TV,T}^\dagger(\varphi_T, \nu) \tilde{\mathbf{b}}_{TV,T}(\varphi'_T, \nu')}{\|\tilde{\mathbf{b}}_{TV,T}^\dagger(\varphi_T, \nu)\| \|\tilde{\mathbf{b}}_{TV,T}(\varphi'_T, \nu')\|}. \quad (12)$$

Its nominator can be written as

$$\sum_{t=1}^T \tilde{\mathbf{b}}_{TV,T}^t(\varphi_T, \nu) \tilde{\mathbf{b}}_{TV,T}^t(\varphi'_T, \nu') = \left[\mathbf{b}_{TV}(\varphi_T) \odot \mathbf{b}_{TV}^*(\varphi'_T) \right]^\dagger \sum_{t=1}^T e^{j2\pi(\nu' - \nu)t} \boldsymbol{\eta}_T^t, \quad (13)$$

and it only depends on $\Delta\nu$. The denominator of Eq. (12) can be expressed by

$$\|\tilde{\mathbf{b}}_{TV,T}(\varphi_T, \nu)\| = \sqrt{T} \cdot \|\mathbf{b}_{TV}(\varphi_T)\|, \quad (14)$$

and it is independent of ν .

It is well known that the Doppler shifts and the impinging directions of the plane waves may contribute to phase changes at the output of the array. The Doppler shift leads to a phase rotation at the same antenna when it senses at different time instants, while the propagation direction of the plane wave also contributes to a phase change between two antennas. The *periodic* structure of the uniform switching sequence leads to ambiguities in the joint estimation of Doppler and propagation direction. It is because the estimator may find more than one plausible combination of Doppler and angle

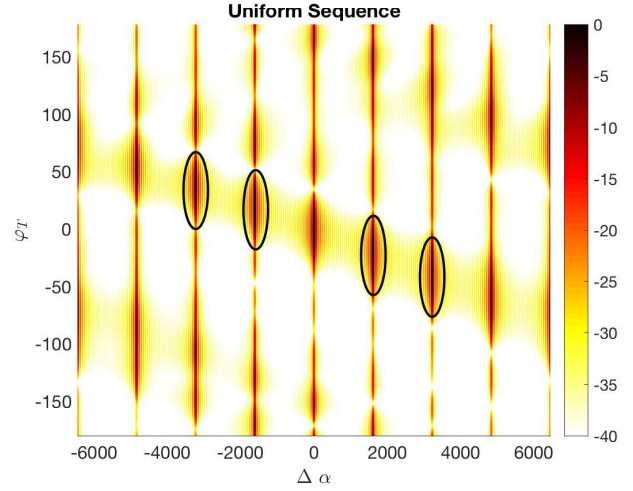


Fig. 1. Amplitude of Ambiguity function (dB) with Azimuth DoD and Doppler shift, under uniform switching schemes at both Tx and Rx

that can produce the phase changes over different antennas and time instants. For example Fig. 1 plots the amplitude upper bound of the ambiguity function given in Eq. (11), when the TX uses the uniform switching pattern. We observe multiple peaks in addition to the central peak located at (0, 0). It also shows that the non-ambiguous estimation range of Doppler is $[-1/2T_0, 1/2T_0]$, when both TX and RX implement uniform switching patterns and $\varphi'_T = 0$. The value of T_0 in this example is $620 \mu\text{s}$ and is based on the transmitted signal in Ref. [11].

III. ALGORITHM

To solve the sequence design problem we need a reasonable metric to evaluate the performance of a particular switching sequence. More importantly we intend to apply the results to wireless channel sounding application, therefore the problem formulation and performance metric should be suitable for real-world arrays.

A. Problem Formulation

The intuitive objective of our array switching design problem is to find schemes that effectively suppress the sidelobes of the spatial-temporal ambiguity function shown in Fig. 1, hence increases the estimation range of Doppler shift. The authors in Refs. [5] and [8] prove that their ambiguity functions have a constant energy, so a preferable scheme should spread the volume under the high sidelobes evenly elsewhere. However the proof again uses the idealized assumption about antenna arrays, thus it cannot be applied directly in our case. Here we introduce the function $f_p(\boldsymbol{\eta}_T)$, which is given by

$$f_p(\boldsymbol{\eta}_T) = \iiint_D |X_T(\varphi_T, \varphi'_T, \Delta\nu)|^p d\varphi_T d\varphi'_T d\Delta\nu, \quad (15)$$

$$D = \{(\varphi_T, \varphi'_T, \Delta\nu) | \varphi_T, \varphi'_T \in (\pi, \pi] \& \Delta\nu \in [0, \nu_{\text{up}}]\}$$

where D is the integration intervals, and ν_{up} represents the target maximal Doppler shift within which we want to avoid

the ambiguity. This value should equal $M_T/2T_0$, because the periodic sequence is only T_0/M_T long. We have conducted numerical simulations based on our proposed ambiguity function in Eq. (11), with the calibrated response of the TX array used in a V2V MIMO channel sounder [11]. Results have shown that its energy, i.e. $f_2(\boldsymbol{\eta}_T)$, is almost constant regardless of the choices of different $\boldsymbol{\eta}_T$. As a result we can use $f_p(\boldsymbol{\eta}_T)$ with a higher value of p as the cost function to penalize the TX switching schemes that lead to high sidelobes. As a summary our optimization problem is given by

$$\begin{aligned} \min_{\mathbf{S}_T \in \mathcal{C}} f_p(\boldsymbol{\eta}_T) \quad (16) \\ \text{s.t. } [\boldsymbol{\eta}_T]_{m_T,t} = ([\mathbf{S}_T]_{m_T,t} - 1)t_1 + (t - 1)M_T t_1, \end{aligned}$$

where the elements in the set \mathcal{C} are integer matrices with a dimension of $M_T \times T$, and every column of \mathbf{S}_T is a permutation of the vector $[1, 2, \dots, M_T]^T$.

B. Solution and Results

Because \mathbf{S}_T takes on discrete values in the feasible set, the simulated annealing algorithm is known to solve this type of problem [12]. The pseudocode of our proposed algorithm is given here in Alg. 1. The key parameters related with this

Algorithm 1 The annealing algorithm to solve our RSAA design problem

- 1: Initialize $\boldsymbol{\eta}_T$, the temperature $T = T_0$, and $\alpha = \alpha_0$;
 - 2: **while** $k \leq k_{\max}$ or $f_p(\boldsymbol{\eta}_T) > \epsilon_{th}$ **do**
 - 3: $\boldsymbol{\eta}'_T = \text{neighbor}(\boldsymbol{\eta}_T)$;
 - 4: **if** $\exp[(f_p(\boldsymbol{\eta}_T) - f_p(\boldsymbol{\eta}'_T))/T] > \text{random}(0, 1)$ **then**
 - 5: $\boldsymbol{\eta}_T = \boldsymbol{\eta}'_T$
 - 6: **end if**
 - 7: $T = \alpha T$
 - 8: **end while**
-

algorithm are $p = 6$, the initial temperature is $T_0 = 100$, the cooling rate is $\alpha_0 = 0.97$ and the $k_{\max} = 500$.

The transition probability from switching scheme (state) $\boldsymbol{\eta}_T$ to $\boldsymbol{\eta}'_T$ is chosen as

$$P_r(\boldsymbol{\eta}_T, \boldsymbol{\eta}'_T) = \begin{cases} \frac{1}{A} \min(1, \exp(\frac{f_p(\boldsymbol{\eta}_T) - f_p(\boldsymbol{\eta}'_T)}{T})), & \text{if } \boldsymbol{\eta}'_T \sim \boldsymbol{\eta}_T \\ 1 - \frac{1}{A} \sum_{\boldsymbol{\eta}''_T \sim \boldsymbol{\eta}_T} \min(1, \exp(\frac{f_p(\boldsymbol{\eta}_T) - f_p(\boldsymbol{\eta}''_T)}{T})), & \text{if } \boldsymbol{\eta}'_T = \boldsymbol{\eta}_T \\ 0, & \text{otherwise} \end{cases} \quad (17)$$

where $\boldsymbol{\eta}'_T \sim \boldsymbol{\eta}_T$ denotes that $\boldsymbol{\eta}'_T$ and $\boldsymbol{\eta}_T$ only differ by swapping two elements in the same column. A is the cardinality of the set $\{\boldsymbol{\eta}'_T | \boldsymbol{\eta}'_T \sim \boldsymbol{\eta}_T\}$, i.e. $A = T \binom{M_T}{2}$.

Fig. 3 provides the values of the objective function with the iteration number and decreased temperature in the SA algorithm. We present the amplitude of the 2D ambiguity function (the upper bound given in Eq. (11)) with the final switching sequence in Fig. 2, where the high sidelobes clearly disappear in contrast with Fig. 1. Another useful metric is the

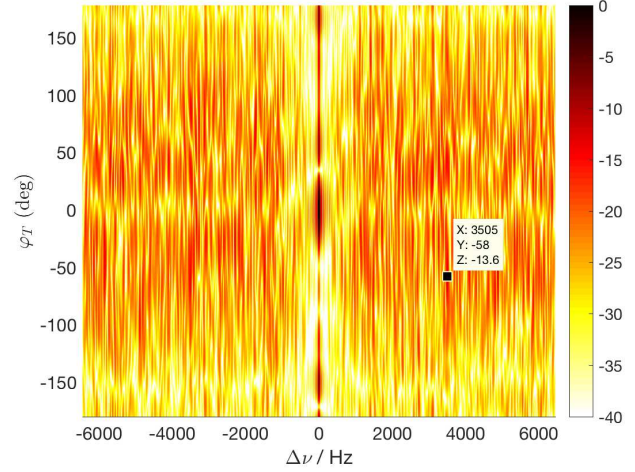


Fig. 2. Amplitude of Ambiguity function with Azimuth DoD and Doppler shift, under uniform Rx switching and scrambled Tx switching scheme

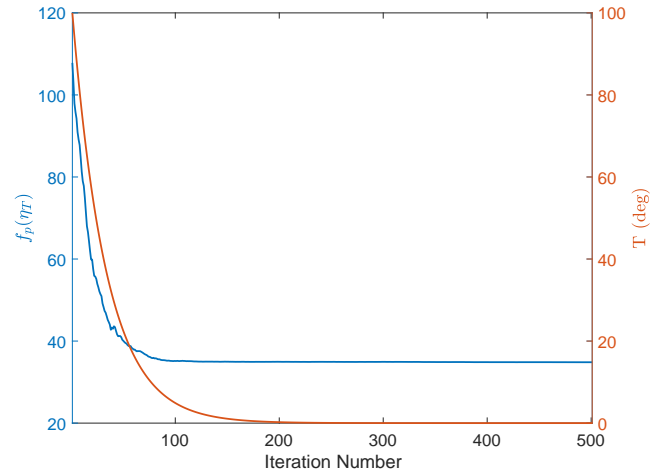


Fig. 3. The evolution of $f_6(\boldsymbol{\eta}_T)$ and temperature during the annealing algorithm in Algorithm 1

NSL used in Ref. [4] to measure the quality of the switching sequence. The NSL here is -13.60 dB, where the lowest value provided in Ref. [4] is -11.06 dB.

IV. NUMERICAL SIMULATIONS

In this section we use Monte Carlo simulations to validate the choice of the switching sequence by investigating the RMSEs of some key parameters, such as azimuth DoD and Doppler shift. We also manage to incorporate $\boldsymbol{\eta}_{T,f}$ into an HRPE algorithm based on the framework of RiMAX, for more details see Ref. [10]. As a comparison we also investigate the case when the same channel is sampled with uniformly switched arrays and evaluated with the corresponding HRPE algorithm in Ref. [9].

For clarity of definitions, we analyze an environment with a single SP, whose parameters are listed in Tab. I. To cover several cases of interest, $|\nu|$ is larger than $1/2T_0 \approx 806$ Hz in snapshot 1 and smaller than $1/2T_0$ in snapshot 2. We compare

TABLE I
PATH PARAMETERS OF ONE-PATH SCENARIO, WHICH SERVES TO VERIFY
THE RMSES OF φ_T AND ν

Snapshot	τ (ns)	φ_T (deg)	φ_R (deg)	ν (Hz)
1	601.1	11.5	59.6	4032.3
2	1117.3	21.3	160.0	80.6

TABLE II
PARAMETER ESTIMATION FOR A TWO-PATH CHANNEL WITH $\eta_{T,f}$,
TRUE/ESTIMATE

Path ID	τ (ns)	φ_T (deg)	φ_R (deg)	ν (Hz)	$ \gamma ^2$ (dB)
1	646.2/646.2	67.81/67.79	-59.33/-59.33	3225.8/3225.8	-13.13/-13.13
2	1203.7/1203.7	-60.15/-60.15	-123.79/-123.78	3217.7/3217.8	-18.82/-18.82

the simulated RMSEs with the squared root of CRLB as a function of signal-to-noise ratio (SNR) ρ for two switching sequences, which are the uniform sequence $\eta_{T,u}$ and our optimized scrambled TX sequence $\eta_{T,f}$. We simulate 1000 realizations at each SNR value. The theoretical CRLB can be determined based on Fisher Information Matrix (FIM) and given by

$$\sigma_{\theta_s}^2 \succeq \text{diag}(\mathcal{J}^{-1}(\theta_s)), \quad (18)$$

where \succeq is the generalized inequality for vectors. Figs. 4 and 5 provide such a comparison for $\eta_{T,f}$, which demonstrates its good performance in both channels with high or low Doppler. On the other hand, Fig. 6 shows the poor estimation accuracy in the high Doppler case for the case of uniform switching pattern $\eta_{T,u}$, although the mean squared error (MSE) can achieve CRLB in the low Doppler scenario as expected in Fig. 7.

We also shown in Fig. 8 the delay-Doppler spectrum of snapshot 1 with three different TX switching sequences, which are $\eta_{T,u}$, $\eta_{T,d}$ (known as the ‘‘dense’’ uniform sequence), and $\eta_{T,f}$. As a result, the spectrum in Fig. 8(a) displays multiple peaks in the same delay bin but at different Doppler shifts, while Fig. 8(c) shows that $\eta_{T,f}$ successfully eliminates all the peaks except for one at the desired location. Notice that $\eta_{T,f}$ also helps distribute the power under those unwanted peaks equally across Doppler. Fig. 8(b) shows that with $\eta_{T,d}$, we can also eliminate the repeated main peaks (and achieve slightly lower sidelobe energy); however, at the price of the separation time between adjacent MIMO snapshots is reduced to $1/8$ of T_0 in $\eta_{T,u}$, which would imply that the number of antenna elements would have to be reduced such that $M_T M_R$ decreases by a factor of 8.

Besides we simulate a two-path channel, which is the simplest version of the multipath channel. Tab. II provides a comparison between the true and estimated parameters where we apply $\eta_{T,f}$ and the newly developed HRPE algorithm. Although both paths’ Doppler shifts are larger than $1/2T_0$, the simulation suggests that the estimated parameters are pleasingly close to the true values.

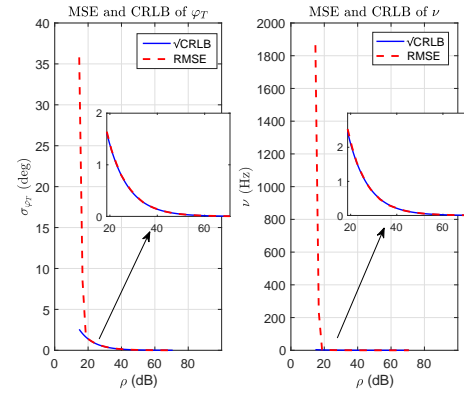


Fig. 4. Comparison about RMSE of φ_T and ν based on Monte-Carlo simulations with the theoretical CRLB from Eq. (18) for snapshot 1 in Tab. I for our scrambled switching pattern.

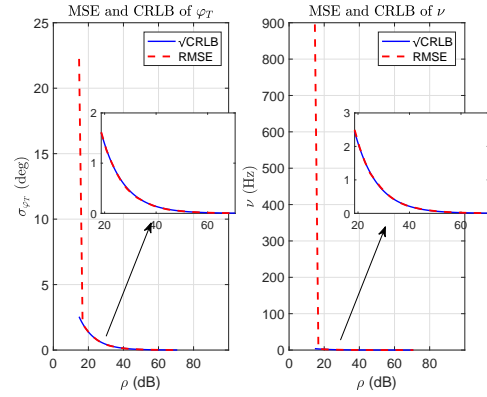


Fig. 5. Comparison about RMSE of φ_T and ν based on Monte-Carlo simulations with the theoretical CRLB from Eq. (18) for snapshot 2 in Tab. I for our scrambled switching pattern.

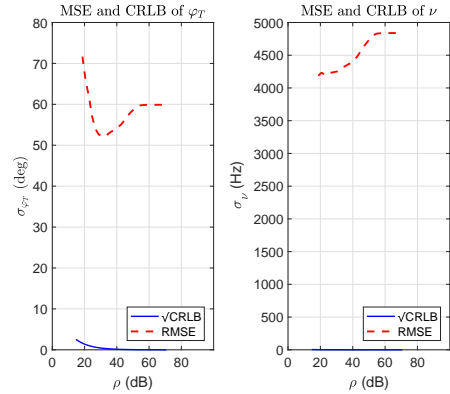


Fig. 6. Comparison about RMSE of φ_T and ν based on Monte-Carlo simulations with the theoretical CRLB from Eq. (18) for snapshot 1 in Tab. I for uniform switching pattern.

V. CONCLUSION

In this paper we revisit the array switching design problem and focus on its adaptability to realistic arrays deployed in channel sounders for fast time-varying channels. We formulate

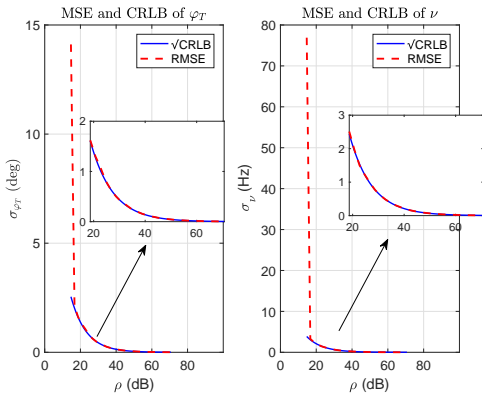


Fig. 7. Comparison about RMSE of φ_T and ν based on Monte-Carlo simulations with the theoretical CRLB from Eq. (18) for snapshot 2 in Tab. I for uniform switching pattern.

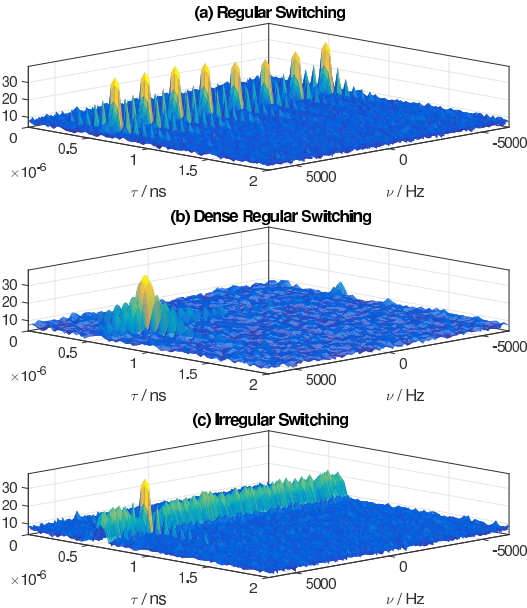


Fig. 8. Delay-Doppler spectrum of snapshot 1 with large Doppler under different TX switching sequences, (a) $\eta_{T,u}$ (b) “dense” uniform sequence (c) $\eta_{T,f}$

the switching design problem as an optimization problem to suppress the sidelobes of the spatio-temporal ambiguity function, which is dependent on array switching patterns. We also show through Monte-Carlo simulations that a RiMAX-based HRPE algorithm where the new sequence is incorporated can produce accurate Doppler and angular estimates in both high and low Doppler scenarios. In the future we will further validate this method and implement related results in applications such as V2V or mmWave MIMO channel measurements.

ACKNOWLEDGMENT

This work was supported by grants from Caltrans, the National Institute of Standards and Technology and the National Science Foundation.

REFERENCES

- [1] A. F. Molisch, *Wireless Communications*, 2nd ed. IEEE Press - Wiley, 2010.
- [2] X. Yin, B. H. Fleury, P. Jourdan, and A. Stucki, “Doppler frequency estimation for channel sounding using switched multiple-element transmit and receive antennas,” in *Global Telecommunications Conference, 2003. GLOBECOM'03. IEEE*, vol. 4. IEEE, 2003, pp. 2177–2181.
- [3] B. H. Fleury, X. Yin, P. Jourdan, and A. Stucki, “High-resolution channel parameter estimation for communication systems equipped with antenna arrays,” in *Proc. 13th Ifac Symposium on System Identification (syst 2003)*, 2003.
- [4] T. Pedersen, C. Pedersen, X. Yin, B. H. Fleury, R. R. Pedersen, B. Bozinovska, A. Hviid, P. Jourdan, and A. Stucki, “Joint estimation of Doppler frequency and directions in channel sounding using switched Tx and Rx arrays,” in *Global Telecommunications Conference, 2004. GLOBECOM'04. IEEE*, vol. 4. IEEE, 2004, pp. 2354–2360.
- [5] T. Pedersen, C. Pedersen, X. Yin, and B. H. Fleury, “Optimization of spatiotemporal apertures in channel sounding,” *Signal Processing, IEEE Transactions on*, vol. 56, no. 10, pp. 4810–4824, 2008.
- [6] F. Belloni, A. Richter, and V. Koivunen, “Doa estimation via manifold separation for arbitrary array structures,” *IEEE Transactions on Signal Processing*, vol. 55, no. 10, pp. 4800–4810, 2007.
- [7] M. Erić, A. Zejak, and M. Obradović, “Ambiguity characterization of arbitrary antenna array: Type I ambiguity,” in *Spread Spectrum Techniques and Applications, 1998. Proceedings., 1998 IEEE 5th International Symposium on*, vol. 2. IEEE, 1998, pp. 399–403.
- [8] C.-Y. Chen and P. Vaidyanathan, “MIMO radar ambiguity properties and optimization using frequency-hopping waveforms,” *Signal Processing, IEEE Transactions on*, vol. 56, no. 12, pp. 5926–5936, 2008.
- [9] R. Wang, O. Renaudin, C. U. Bas, S. Sangodoyin, and A. F. Molisch, “High resolution parameter estimation for time-varying double directional V2V channel,” *IEEE Transactions on Wireless Communications*, vol. PP, no. 99, pp. 1–1, 2017.
- [10] R. Wang *et al.*, “Optimal array switching sequence for the TDM channel sounding in a fast time-varying channel,” To be submitted.
- [11] R. Wang, C. U. Bas, O. Renaudin, S. Sangodoyin, U. T. Virk, and A. F. Molisch, “A real-time MIMO channel sounder for vehicle-to-vehicle propagation channel at 5.9 GHz,” in *Communications (ICC), 2017 IEEE International Conference on*. IEEE, 2017, pp. 1–6.
- [12] S. Kirkpatrick, C. D. Gelatt, M. P. Vecchi *et al.*, “Optimization by simulated annealing,” *science*, vol. 220, no. 4598, pp. 671–680, 1983.